

# Dynamic plane strain testing as an alternative method to characterise cyclic direct simple shear experiment on sands

R. Banerjee<sup>1</sup>, Y.M. Parulekar<sup>1</sup>, A. Sengupta<sup>2</sup>, J. Chattopadhyay<sup>1</sup>

<sup>1</sup>*Bhabha Atomic Research Centre & Homi Bhabha National Institute, Mumbai, India*

<sup>2</sup>*Department of Civil Engineering, Indian Institute of Technology, Kharagpur, India*

**ABSTRACT:** A numerical investigation on a sand under plane strain condition subjected to a cyclic loading on a shake table has been described to characterise the stress conditions during a cyclic direct simple shear (DSS) experiment. The objective is to develop a reliable plane strain dynamic test facility for soils which can replicate essential dynamic behaviours of a sand observed in a standardized test. A laboratory plane strain cell of dimension 226mm x 146mm x 25mm has been fabricated in-house which is to be mounted on a 5 tonnes capacity uniaxial shake table. The nonlinear dynamic effective stress analyses of the undrained plane strain tests are performed using an advanced constitutive model, PM4Sand and the results are compared with the published results of actual cyclic direct simple shear (DSS) experiments on Ottawa F65 sand in terms of stress-strain behaviour and the effective stress path. It is observed that there is a good qualitative agreement of the stress path obtained from the plane strain dynamic analyses and the cyclic DSS tests. Additional numerical analyses have been conducted using sinusoidal motions of varying amplitude and frequency to gain an insight into the extent of cyclic mobility of a sand with amplitude and frequency.

**Keywords:** Plane strain; Shake table; Cyclic DSS; PM4Sand.

## 1 INTRODUCTION

In a site response analysis, it is observed that the frequency components of an input motion are amplified which are near to the natural frequency of the soil deposits or its higher harmonics, and the high frequency contents are reduced (Kramer, 1996). If the soil is saturated or liquefiable, it is observed that an input motion is de-amplified or insulated near the top surface. Interestingly, it is observed in some cases (Bradley, 2012) that a liquefied soil instead of de-amplifying, it amplified the ground motion in the form of distinct peaks. Zeghal and Elgamal (1998) has linked the distinct peaks of a response acceleration with a sudden drop in the pore water pressure response. The study attributes the spikes in the acceleration to the phenomena of cyclic mobility of a saturated sand after initial liquefaction. But a question remains regarding the circumstance that leads to a spike in a response acceleration. This has been investigated by Wang et al. (2018) who concluded that if an input displacement is large enough to overcome the “fluid like shear strain” in each cycle, then one may expect the phenomena of cyclic mobility (or a sudden spike in a response acceleration).

The main objective of this study is to develop a reliable plane strain dynamic test facility for soils as most of the dynamic analyses assumes a plane strain condition in the soil mechanics. A laboratory plane strain cell of dimension 226mm x 144mm x 25mm has been fabricated in-house to be mounted on a uni-axial shake table

for soil testing under 1-g environment. A detailed pre-test numerical simulation of a saturated sand within the dynamic plane strain cell is performed to investigate the basic phenomena of pre and post liquefaction behaviour of the saturated sand. The results (in terms of stress-strain response, effective stress paths) are compared with the standardized cyclic direct simple shear (CDSS) test results conducted on Ottawa F65 sand by El Ghoraiby et al. (2021) as a part of international LEAP-2020 project. It is observed that there is a good qualitative agreement between the CDSS test results and the pre-test numerical simulations. Additional numerical analyses have been conducted with varying frequency and amplitude of the base motion to investigate the extent of cyclic mobility (or pre and post liquefaction behaviour).

## 2 CALIBRATION OF MODEL PARAMETERS FOR THE SAND

The constitutive model used for the sand is PM4Sand (Ziotopoulou and Boulanger, 2013), a critical state, bounding surface plasticity model. It is well equipped to capture the monotonic and the cyclic behaviour of a sand under drained and undrained conditions. The calibration is performed with the available monotonic triaxial test data on Ottawa F65 sand (El Ghoraiby et al. 2020) to account for the cyclic strength, stress paths and the post liquefaction shear-strain rate (Tasiopoulou et al. 2019)

of the sand by constraining the critical state line (CSL). The primary model parameters are apparent relative density ( $D_{Ro}$ ) ( $= 0.67$ ), the shear modulus coefficient ( $G_o$ ) ( $= 580$  kPa to match with the small strain shear modulus ( $G_{max}$ ) reported by El Ghoraiby et al. 2020), the contraction rate parameter,  $h_{po}$  ( $= 0.07$ , obtained iteratively to match the liquefaction resistance curve of Ottawa F65 sand). The secondary model parameters which are modified to get a proper post liquefaction response (or cyclic mobility) are maximum void ratio,  $e_{max}$  and minimum void ratio,  $e_{min}$  which are 0.78 and 0.51, respectively (El Ghoraiby et al. 2020). Q and R parameters of the empirical CSL curve are calibrated to match the results of the monotonic triaxial tests on Ottawa F65 sand and found to be 10 and 1.1 (Figure 1). The bounding surface constant,  $n_b$  and the value of the plastic modulus,  $h_o$  are assumed as 0.4 and 0.3, respectively to match the post liquefaction shear strain rate accumulation. The calibrated model parameters of PM4Sand are listed in Table 1.

Table 1. Calibration of PM4Sand parameters

Parameters	Value	Description
$G_o$	580	Used in small strain modulus
$h_{po}$	0.07	Contraction rate
$n_b$	0.4	Bounding surface constant
$\phi_{cv}$	$30^\circ$	Constant volume friction angle
$e_{max}, e_{min}$	0.78, 0.51	Parameters for Ottawa F65 sand
Q	10	CSL constant for Ottawa F65 sand
R	1.1	CSL constant for Ottawa F65 sand
$h_o$	0.3	Plastic modulus parameter

The other model parameters are assigned default values given by Ziotopoulou and Boulanger (2013).

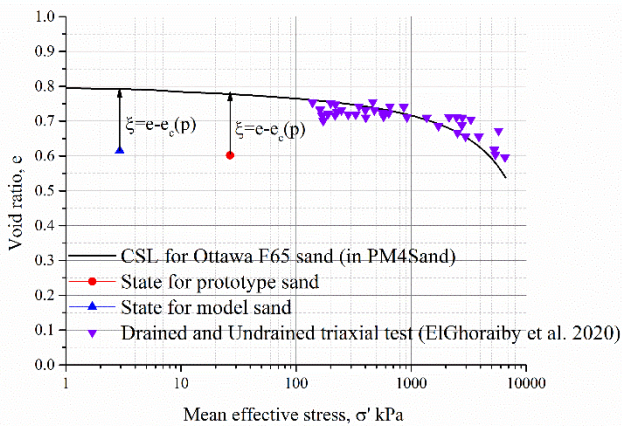


Figure 1. Calibrated CSL line along with the monotonic triaxial tests on Ottawa F65 sand.

Figure 2 shows the liquefaction resistance curve obtained from numerical simulation, the curve proposed by Boulanger and Idriss (2014) and the results from CDSS experiments conducted on Ottawa F65 sand under a vertical effective pressure of 40 kPa. Figure 3 shows the comparison of the experimental data and the numerical simulation of Ottawa F65 sand in terms of stress-strain curve and effective stress paths for a cyclic stress ratio (CSR) of 0.16. These calibrated parameters are utilized to obtain the response of the sand in a plane strain cell subjected to a harmonic motion at the bottom.

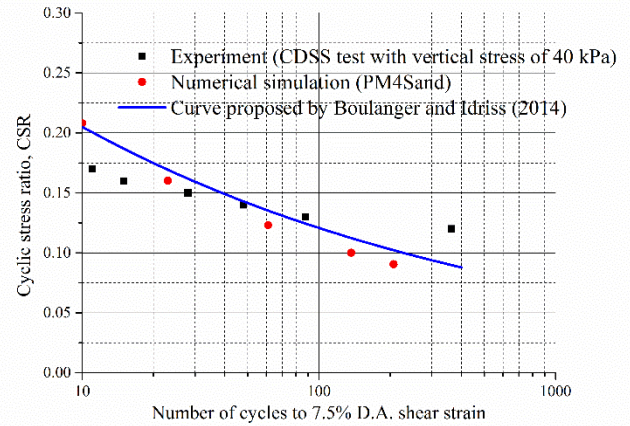


Figure 2. Calibrated liquefaction resistance curve obtained from PM4Sand, curve proposed by Boulanger and Idriss (2014) along with the laboratory strength curve of Ottawa F65 sand.

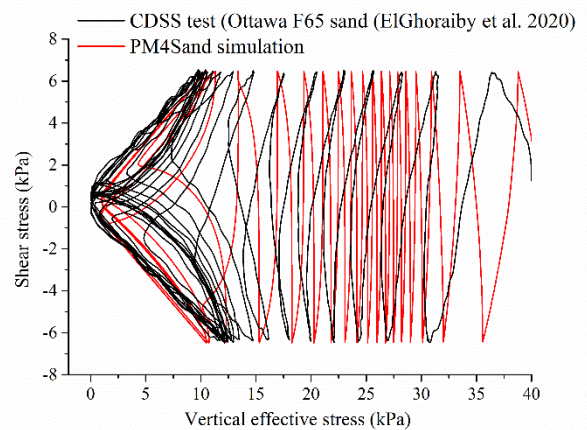
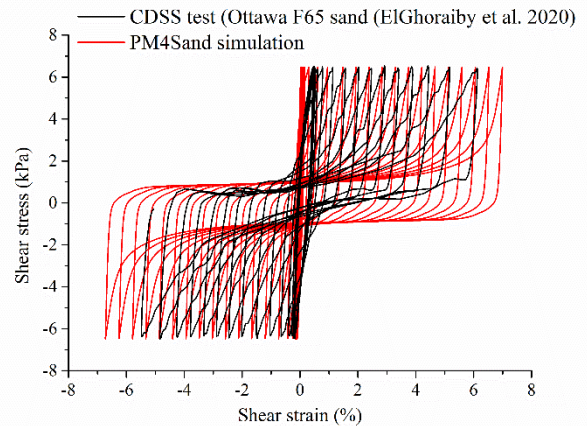


Figure 3. Numerical simulation of CDSS test compared with the experiment on Ottawa F65 sand for a CSR value of 0.16.

### 3 DETAILS OF A PLANE STRAIN APPARATUS ON A 1-G SHAKE TABLE

In the present work, a laboratory plane strain cell made of 226mm x 144mm x 25mm Perspex plates has been developed in-house. The details of the plane strain apparatus is elaborated in Sengupta (2010). The plane strain cell is planned to be mounted on a 5 tonnes uniaxial shake table comprised of a 1m x 1m steel table mounted on rails. The table is attached to a servo hydraulic actuator driven by a controller. The controller is capable of accepting earthquake motions with frequencies ranging from 0.01 Hz to 50 Hz. The schematic diagram of the plane strain cell mounted on a shake table is shown in Figure 4. Three accelerometers are embedded inside the saturated sand sample from which shear stresses and shear strains are back calculated following the procedure of Zeghal and Elgamal (1994). The average pore pressure inside the plane strain sample is measured by a pore pressure transducer. Lateral confining pressures are applied by inflating balloons located inside side chambers by an air compressor as shown in Figure 4. The entire apparatus is to be mounted on the shake table and subjected to sinusoidal motions of various amplitude and frequencies to investigate the phenomena of cyclic mobility and to compare with the actual CDSS experimental results.

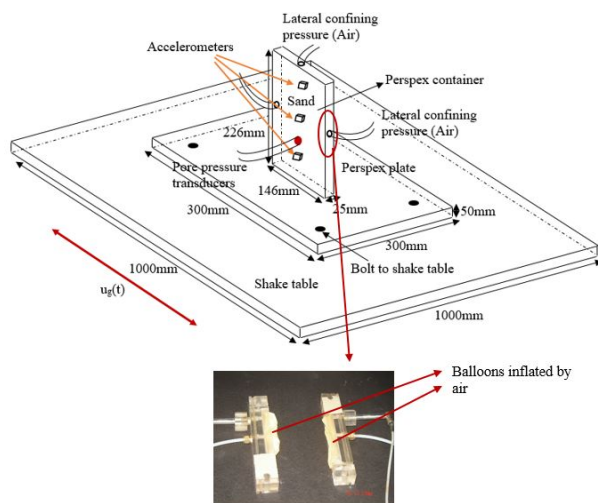


Figure 4. Schematic diagram of dynamic plane strain test setup.

### 4 NONLINEAR 2D DYNAMIC ANALYSES OF SAND IN PLANE STRAIN CONDITION

The numerical simulation follows the 1-g scaling law proposed by Wood (2004). The scale factor assumed in this study to relate the model and the prototype parameters is 9.0. The scale factor for mass density is not 1.0, since it is necessary to replicate the geometrically similar stress paths (in  $\tau$  (shear stress)- $\sigma'$  (mean effective stress) plane) of the model and the prototype sand. This is done by keeping the initial state parameter,  $\xi = e -$

$e_c(p)$  of the sand constant in both the model and the prototype (Roscoe and Poorooshasb, 1963; Banerjee et al. 2022) as shown in Figure 1. Table 2 explains the scaling of relevant parameters used in the numerical simulation. All the plane strain 2D numerical simulations have been performed on a prototype scale and the corresponding results have been compared with the results of CDSS experiments conducted by El Ghoraiby et al. (2021).

Table 2. Scaling in 1-g environment (Wood 2004).

System variables	Geometric scaling factor	Prototype	Model (In 1-g env.)
Void ratio (or relative density)	Equaling state parameter ( $e_c(p)$ ) from CSL of Ottawa F65 sand	0.602 (71.3%)	0.6149 (67.06%)
Dry unit weight ( $\lambda_p$ ) (*)	1.0080	16.2275 kN/m <sup>3</sup>	16.0973 kN/m <sup>3</sup>
Acceleration ( $\lambda_g$ )	1	1	1
Length ( $\lambda_L$ )	9 (assumed)	1.314m, 2.034m	0.146m, 0.226m
Stress ( $\lambda_s$ )	9.07533 ( $\lambda_p \lambda_g \lambda_L$ )	40 kPa, 20 kPa	4.407kPa, 2.204 kPa
Modulus ( $\lambda_G$ )	3.01253 ( $\sqrt{\lambda_s}$ ) (since $G \propto \sqrt{\sigma}$ , $G = G_o \frac{(2.97-e)}{(1+e)} \sqrt{\frac{\sigma}{p_{atms}}}$ )	Variable (depend on the variation of G value with confg. stress)	Variable (depend on the variation of G value with confg. stress)
Strain ( $\lambda_s / \lambda_G$ )	3.01253		
Time (dynamic) ( $\lambda_L (\lambda_p / \lambda_G)^{0.5}$ )	5.20699	16 sec, 6 sec, etc.	3.073 sec, 1.152 sec, etc.
Frequency ( $(\lambda_G / \lambda_p)^{0.5} / \lambda_L$ )	0.17743	1 Hz, 3 Hz, etc.	5.64 Hz, 16.91Hz, etc.
Pore fluid density	1.0	10	10
Pore pressure ( $\lambda_p \lambda_L$ )	9.07533	Variable with depth	Variable with depth

\* The scaling of density is not 1.0 (=1.008) since the void ratio for the model and the prototype are not same.

A two dimensional, nonlinear, undrained (no flow condition) dynamic analysis of the sand within the plane strain cell (on a prototype scale) is performed using a commercial software MIDAS FEA NX (2021). A schematic diagram of the dynamic analysis of the sand within the plane strain apparatus along with the measurement locations of the acceleration, stress-strain, etc. are shown in Figure 5.

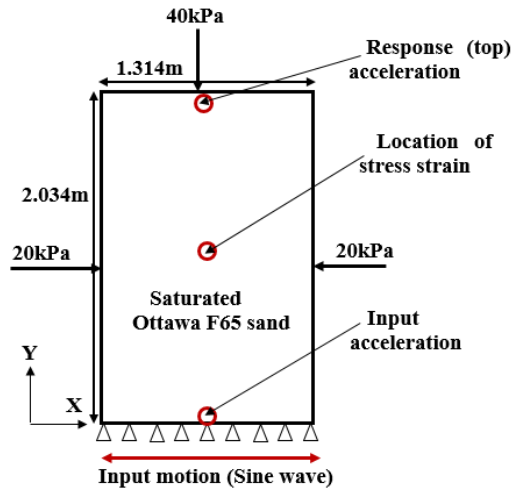


Figure 5. Schematic diagram of the sand sample within the dynamic plane strain apparatus along with the measurement locations of stresses, strains and accelerations (in prototype scale).

The soil sample of dimension 1.314m (in width) x 2.034m (in height) is discretized by 4-noded plane strain quadrilateral elements, each of size 0.678m x 0.438m, keeping in mind the maximum frequency (20 Hz) that each finite element grid is able to transmit. In the static analysis, the soil sample is subjected to a confining pressure of 40 kPa on the vertical boundary and 20 kPa on the lateral boundaries. The bottom nodes of the soil is fixed in both, x- and y-directions. The sand is modelled as Mohr-Coulomb model with the elastic and the plastic properties in line with that listed by El Ghoraiby et al. (2020) and it is allowed to equilibrate. The bulk modulus of water is assumed to be zero in the static phase. After performing the initial static analysis, the dynamic analysis is performed. In the dynamic analysis, the soil model is changed to PM4Sand with the properties listed in Table 1, and acceleration time history is assigned to all the bottom nodes in the horizontal (x) direction keeping the bottom nodes fixed. The degree of freedom of the top nodes are tied in both, x and y, directions during the dynamic analysis and the stress-strain, effective stress paths and the acceleration time history are obtained. It is to be noted that if the degree of saturation ( $S$ ) is less than unity, then the pore pressure is not calculated for an element. It is a common practise to modify the bulk modulus of water to take into account the degree of saturation (Biot, 1962; Banerjee et al. 2021). Since the degree of saturation is not known beforehand, it is assumed that the degree of saturation is unity ( $S=1$ ) which corresponds to the value of  $2 \times 10^9$  Pa for the bulk modulus of water during the dynamic analysis. The small strain damping is assumed to be 0.75% with the predominant frequency of the input motion.

Figure 6 shows a direct comparison between the stress-strain response and the effective stress path obtained from the numerical simulation (with 16 secs of

0.2g sinusoidal wave at 1 Hz frequency) and the results of CDSS experiment with CSR value of 0.35 with non-uniform shear stress amplitude. A reasonable qualitative agreement between the numerical and the experimental results is observed, which gives confidence in the present analyses procedure. The un-symmetrical response of the stress- strain in the CDSS experiment is attributed to the initial static shear stress ( $\tau_{\text{initial}}$ ) which is applied to mimic the initial conditions on a slope subjected to a gravity loading. Since there is no initial static shear stress on the sand in the plane strain apparatus, the response is symmetrical in nature. To simulate the initial static shear stress in the soil sample and to properly compare with the CDSS test results, the top slope of the soil and the top platen of the plane strain cell have to be sloped by approx.  $4-5^\circ$ . This will introduced an unsymmetrical stress-strain field in the soil sample.

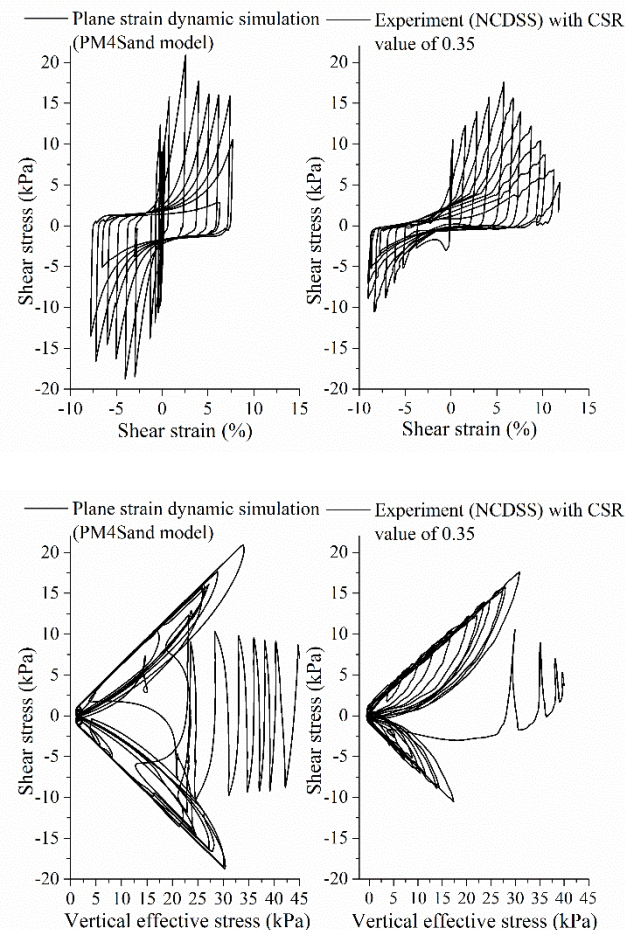


Figure 6. Comparison of the stress-strain, effective stress paths obtained from 2D numerical simulation and CDSS experiment conducted on Ottawa F65 sand.

Figure 7 shows a comparison between the input acceleration and the response acceleration in which spikes are observed after 7 secs of motion, which is a signature of cyclic mobility. These spikes are related to the strain hardening behaviour at non-zero effective stress. The enlargement of the time interval between the two spikes is associated with the “fluid like shear strain”

which occurs near zero effective stress (Wang et al. 2018).

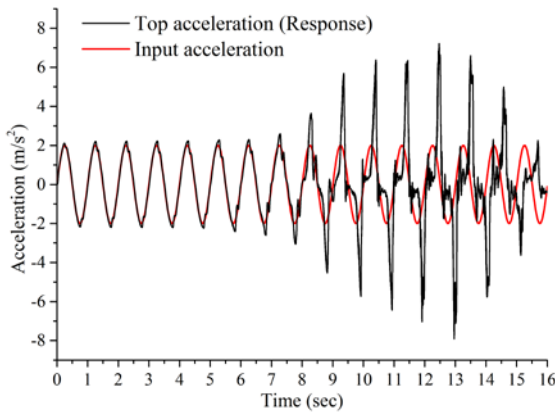


Figure 7. Input sine wave of 0.2g PGA with 1 Hz frequency (applied for 16 cycles) and the response acceleration (in prototype scale) at the top of the sand sample.

To investigate the effect of input frequency on the soil behaviour (i.e., extent of cyclic mobility), the same soil is now subjected to 16 secs of 0.2g input motion at 1 Hz frequency and 4 secs of same motion at 4 Hz frequency (i.e., 16 cycles). The responses in terms of acceleration, stress-strain and effective stress path are shown in Figures 7, 8 and 9. It is observed that the response acceleration after 1 sec eventually vanished for the 4 Hz motion. This is in line with the stress- strain response and the effective stress paths oscillating close to zero. This is because of the “fluid like shear strain”. At this instance, the sand is basically shearing near zero effective stress and cannot transfer any shear force to the top due to which the response acceleration through the sand is insulated. It is also observed that the soil vibrates out of phase with respect to the input motion in Figure 8 after 1 sec. This phenomenon occurs when there is a non-exceedance of “fluid like shear strain” in each cycle. Hence, if the input frequency is changed keeping the amplitude same, the pre- and post-liquefaction phases of the sand behaviour is modified accordingly.

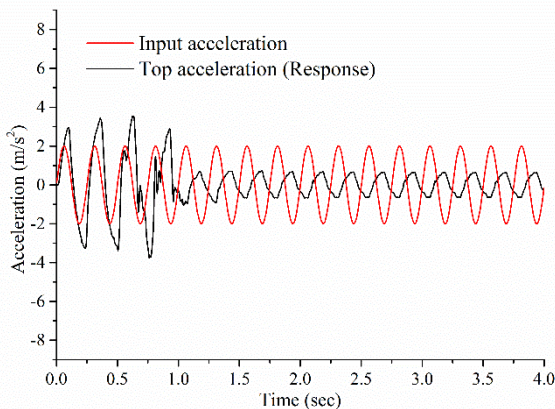


Figure 8. Input sine wave of 0.2g PGA with 4 Hz frequency (applied for 16 cycles) and the numerically obtained response acceleration.

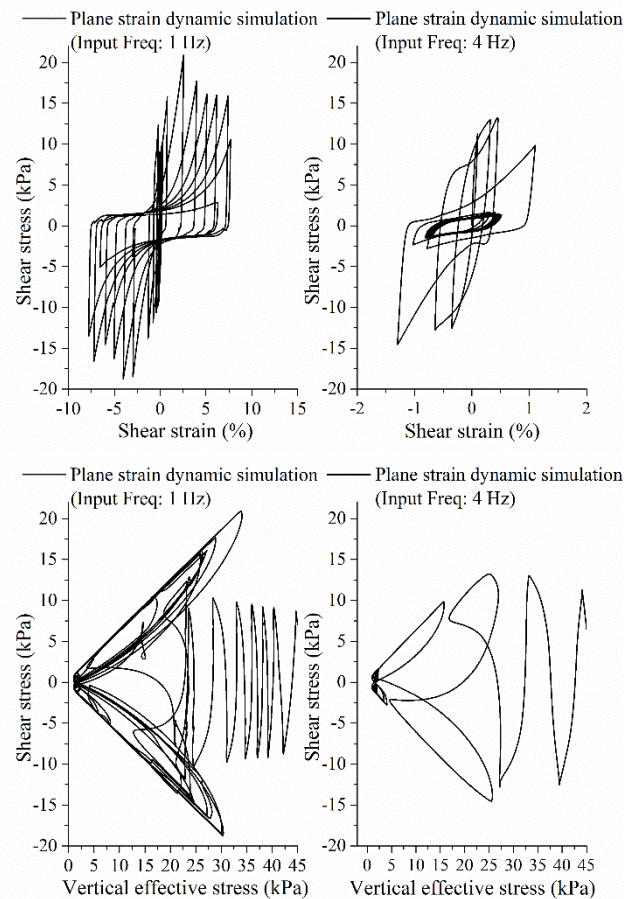
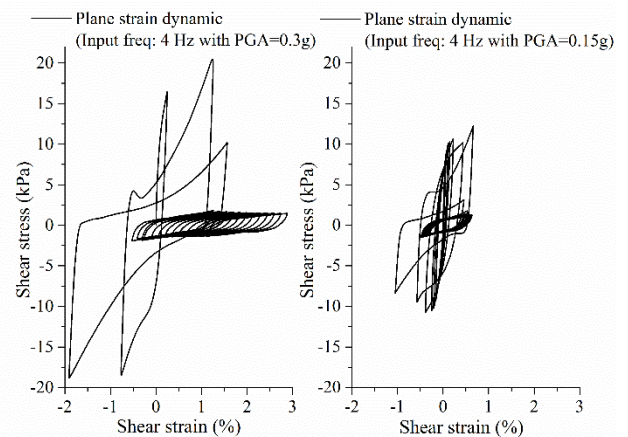


Figure 9. Stress-strain and effective stress path from numerical analyses for 16 cycles of sine wave of 0.2g amplitude with frequency of 1 Hz and 4 Hz.

To investigate the effect of the amplitude of the input motion keeping the same frequency, the soil is subjected to two different amplitude of input motions namely, 0.15g and 0.3g with 4 Hz frequency. The responses in terms of stress-strain and the effective stress paths are shown in Figure 10. It is observed that the pre-liquefaction phase of the soil is affected and the soil subjected to a larger amplitude of motion gets liquefied earlier.



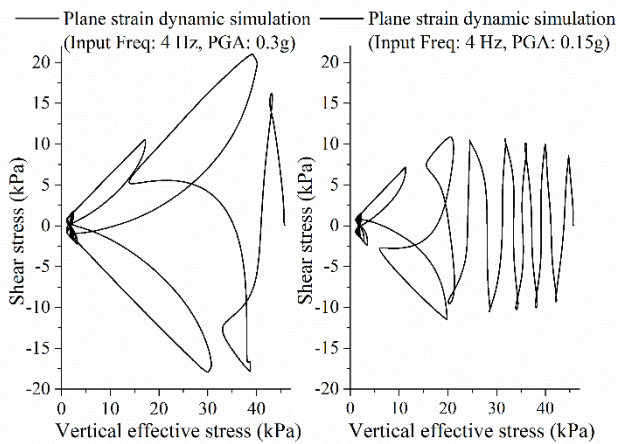


Figure 10. Stress-strain and effective stress paths predicted for 16 cycles of sine wave with amplitude of 0.15g and 0.3g at a frequency of 4 Hz.

## 5 CONCLUSIONS

In the present study, a detailed pre-test numerical analysis of a sand sample within a plane strain apparatus fixed on a uniaxial shake table is presented. A reasonably good agreement between the numerical and the actual CDSS experimental results conducted on Ottawa F65 sand is observed, which gives some confidence on the numerical procedure followed for the pre-test analyses.

A number of additional numerical analyses have been conducted using sinusoidal motions of varying amplitude and frequency to gain an insight into the extent of cyclic mobility of the sand with amplitude and frequency. It is found that if the frequency of the input motion is varied keeping the amplitude constant, both pre- and post-liquefaction behaviour of the sand is affected. But, if the amplitude of the input motion is varied keeping the frequency constant, only the pre-liquefaction regime of the sand is affected.

## 6 ACKNOWLEDGEMENTS

All the data on Ottawa F65 sand has been obtained from the Intl. LEAP-2020 project (doi: 10.17603/ds2-92c9-t496) which is gratefully acknowledged.

## 7 REFERENCES

- Banerjee, R., Chattaraj, R., Sengupta, A., Parulekar, Y.M. 2022. Dynamic behaviour of a piled raft resting on saturated Kasai River sand, *Geomechanics and Geoengineering*, **17**(4), 1023-1055.
- Banerjee, R., Chattaraj, R., Parulekar, Y.M., Sengupta, A. 2021. Numerical prediction of undrained cyclic triaxial experiments on saturated Kasai River sand using two constitutive models of liquefaction, *Bulletin of Engineering Geology and the Environment*, **80**(11), 8565-8582.
- Biot, M.A. 1962. Mechanics of deformation and acoustic propagation in porous media, *J Appl Phys*, **33**, 1482-1498.
- Boulanger, R.W., Idriss, I.M. 2014. CPT and SPT liquefaction triggering procedures. *Report No UCD/GCM-14/01*.
- Bradley, B.A. 2012. Strong Ground Motion Characteristics Observed in the 4 September 2010 Darfield, New Zealand Earthquake, *Soil Dynamics and Earthquake Engineering*, **42**(4), 32-46.
- El Ghoraiby, M., Park, H., Manzari, M.T. 2020. Stress strain behaviour and liquefaction strength characteristics of Ottawa F65 sand, *Soil Dynamics and Earthquake Engineering*, **138**, 106292.
- El Ghoraiby, M., Manzari, M.T. 2021. Cyclic Direct Simple Shear Tests-Uniform Loading, *In LEAP-2020: Cyclic triaxial and Direct Simple Shear Tests Performed at GWU*, Design Safe-CI, <https://doi.org/10.17603/ds2-dyph-pf84v1>.
- El Ghoraiby, M., Manzari, M.T. 2021. Cyclic Direct Simple Shear Tests-Nonuniform Loading, *In LEAP-2020: Cyclic triaxial and Direct Simple Shear Tests Performed at GWU*, Design Safe-CI, <https://doi.org/10.17603/ds2-dwt9-ke80v1>.
- Kramer, S.L. 1996. *Geotechnical Earthquake Engineering*, Prentice-Hall, Upper Saddle River, N.J.
- MIDAS FEA NX. 2021. User Manual.
- Roscoe, K.H., Poorooshasb, H.B. 1963. A fundamental principle of similarity in model tests for earth pressure problems, *Proc. 2<sup>nd</sup> Asian Conf. Soil Mech*, 1,134.
- Sengupta, A. 2010. Strain localization in geomaterials in nature, laboratory tests and numerical analysis, *Current Science*, **98**(9), 1195-1201.
- Tasiopoulou, P., Ziotopoulou, K., Humire, F., Giannakou, A., Chacko, J., Travararou, T. 2020. Development and implementation of semi empirical framework for modelling post liquefaction shear deformation accumulation in sands, *Journal of Geotechnical and Geoenvironmental Engineering, ASCE*, **146**(1), 04019120.
- Wang, G., Xing, W., Zhao, J. 2018. Modelling spiky acceleration response of dilative sand deposits during earthquakes with emphasis on large post-liquefaction deformation, *Earthq Eng & Eng Vib*, **17**, 125-138.
- Wood, D.M. 2004. *Geotechnical modelling*. CRC press, London, UK.
- Zeghal, M., Elgamal, A. 1994. Analysis of site liquefaction using earthquake records, *Journal of Geotechnical Engineering, ASCE*, **20**(6), 996-1017.
- Ziotopoulou, K., Boulanger, R.W. 2013. Calibration and implementation of a sand plasticity plane strain model for earthquake engineering application, *Soil Dynamics and Earthquake Engineering*, **53**, 268-280.